

Machine learning prediction of network dynamics with privacy protection

Xin Xia,¹ Yansen Su,² Linyuan Lü,³ Xingyi Zhang,² Ying-Cheng Lai,⁴ and Hai-Feng Zhang^{1,*}

¹*The Key Laboratory of Intelligent Computing and Signal Processing of Ministry of Education, School of Mathematical Science, Anhui University, Hefei 230601, China*

²*The Key Laboratory of Intelligent Computing and Signal Processing of Ministry of Education, School of Artificial Intelligence, Anhui University, Hefei 230601, China*

³*Institute of Fundamental and Frontier Sciences, University of Electronic Science and Technology of China, Chengdu, 610054, China*

⁴*School of Electrical, Computer and Energy Engineering, Arizona State University, Tempe, Arizona 85287, USA*

(Dated: June 13, 2022)

Predicting network dynamics based on data, a problem with broad applications, has been studied extensively in the past, but most existing approaches assume that the complete set of historical data from the whole network is available. This requirement presents a great challenge in applications, especially for large, distributed networks in the real world, where data collection is accomplished by many clients in a parallel fashion. Often, each client only has the time series data from a partial set of nodes and the client has access to only partial timestamps of the whole time series data and partial structure of the network. Due to privacy concerns or license related issues, the data collected by different clients cannot be shared. To accurately predict the network dynamics while protecting the privacy of different parties is a critical problem in the modern time. Here, we propose a solution based on federated graph neural networks (FGNNs) that enables the training of a global dynamic model for all parties without data sharing. We validate the working of our FGNN framework through two types of simulations to predict a variety of network dynamics (four discrete and three continuous dynamics). As a significant real-world application, we demonstrate successful prediction of State-wise influenza spreading in the USA. Our FGNN scheme represents a general framework to predict diverse network dynamics through collaborative fusing of the data from different parties without disclosing their privacy.

I. INTRODUCTION

This paper deals with the problem of predicting complex network dynamics from distributed data without compromising the privacy of the data sources. In particular, given a large network whose dynamics are unknown but only *local* historical data or time series are available through measurements conducted by different parties (clients or agents), the objective is to accurately predict the dynamical evolution of the network for a number of time steps under the constraint of no data sharing of any kind among the clients. To paraphrase it, among the clients who performed the measurements, there can be no communication of any sort for privacy considerations. This problem of predicting network dynamics without privacy disclosure is significantly more challenging than previously studied inverse problems in the field of reverse engineering of networked dynamical systems. The main contribution of this paper is the articulation and validation of an effective machine learning based solution to this problem.

To infer or reconstruct the dynamical process on a network based on time series data has been an active field in the past two decades [1, 2]. A diverse array of methodologies were proposed, including those based on the collective dynamics [3–7], stochastic analysis [8, 9],

compressive sensing [10–15], and machine learning [16–19]. In nonlinear dynamics, the research on data based identification and forecasting of system dynamics has an even longer history [20, 21]. For example, an earlier approach focused on approximating a nonlinear system by various linear equations in different regions of the phase space so that the local Jacobian matrices can be constructed [20, 22, 23] or the ordinary differential equations can be found to fit the data [24]. Methods based on chaotic synchronization [25] for estimating the system parameters were also investigated. Of particular importance is the approach to finding the system equations (hence the system dynamics) from data. This “natural” approach dated back to the original work of Crutchfield and McNamara [26], who exploited the concept of qualitative information to deduce the effective equations of motion of the system responsible for the deterministic portion of the observed random behavior. An inverse Frobenius–Perron approach to generate a dynamical system close to the original system in the sense of the invariant density was proposed [27]. The Kronecker product representation was also used for modeling and nonlinear parameter estimation [28]. In the past decade, sparse optimization methods, e.g., compressive sensing [29, 30], was introduced for finding the system equations from data [10–12, 15, 31] for nonlinear and complex dynamical systems whose velocity fields or mapping functions are describable by a number of fairly elementary mathematical functions. This equation-finding approach, while appealing and satisfying from a mathematical point of view,

* haifengzhang1978@gmail.com

may not have significant practical value in real world applications, as the dynamical processes there often cannot be described by a collection of simple functions. Even in cases where an approximate set of equations can be found, sensitivity to small errors typically seen in nonlinear and complex dynamical systems can lead to large deviations between the dynamics as predicted by the equations and the ground truth. In these situations, machine learning has gained recent attention as a viable approach to predicting dynamics from data [17, 18, 32–41].

To our knowledge, the increasingly critical issue of privacy has not been addressed in the literature on data-based prediction of network dynamics. In fact, a tacit assumption employed in the current literature on data-based prediction of network dynamics is that the observed data are transparent and available to all the observers, which include the network structure and the time series data, as schematically illustrated in Fig. 1(a). If all the data are collected by a single client, privacy is not an issue. However, in applications, practical limits such as the cost of observations and the timeliness render necessary employing different clients to collect the data [42]. For example, disease-related data at different times and/or in different regions are often collected by multiple parties, which cannot be shared due to the requirements of data security and privacy protection, leading to the emergence of the so-called “data islands” [43, 44]. In the era of big data analytics and machine learning, data have significant commercial, security, and applied values. While the pertinent entities are able to better accomplish their goals with more data, privacy protection puts a limit on how much data any individual client is able to acquire. For network dynamics, more time series data and more information about the network structure are certainly beneficial to achieving higher accuracies in predicting the dynamical evolution, but the data need to be collected by individual clients for which privacy may be of great importance. A key question with practical significance is how to coordinate the network structure and time series data distributed in different organizations to improve the accuracy of dynamics prediction, without compromising privacy.

Existing cooperative data-learning methods include secure multiparty computing [45], multitask learning [46], and federated learning [47]. As a distributed machine learning technology with privacy protection where data fusion can be achieved among the parties without leaking their private data [48], federated learning has gained much interest in applications such as traffic flow prediction [49] and recommendation systems [50]. Federated learning has also been exploited for graph representation learning [51, 52] and its downstream tasks such as node classification, link prediction, and graph classification [53–55]. The basic principle underlying federated learning is that each client trains a local model with local data, and a joint global model is generated by aggregating the parameters of the local models [56]. Whether the federated learning framework can predict the network dy-

namics and how to use it to predict the network dynamics based on multiparty data have not been considered. To this end, we set out to develop a framework based on Federated Graph Neural Networks (FGNNs) to predict the network dynamics from distributed time-series data through jointly learning an optimal global dynamics model without exposing the data of each party, i.e., without compromising privacy.

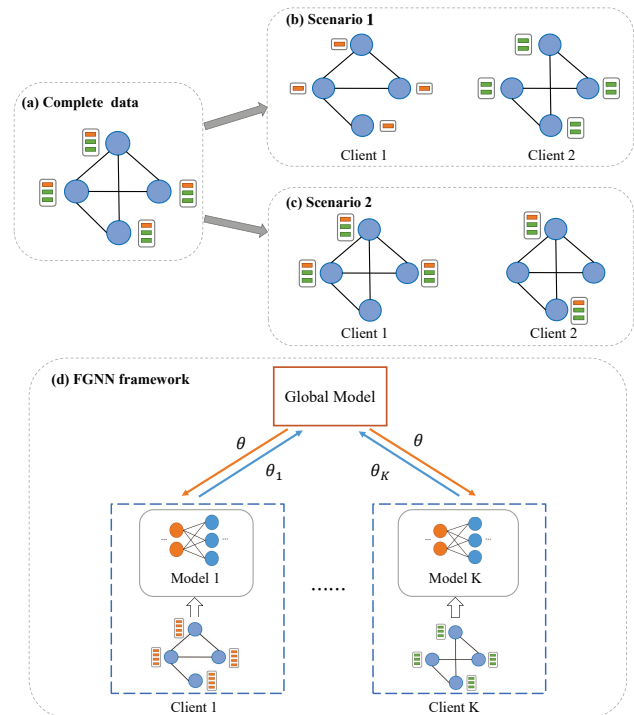


FIG. 1. Scenarios of multiparty data collection and the proposed FGNN framework for predicting the network dynamics without compromising privacy. (a) Data collection without privacy protection. Clients 1 and 2 are two local clients. The rectangular boxes represent the time series data of the nodes with the color of the box indicating the data at different timestamps. In this case, each client has complete time series data of the nodes and complete information about the network structure, so the information possessed by both clients is transparent to each other, i.e., no privacy. (b) Each client collects only partial timestamps of the time series data with incomplete knowledge about the network structure (Scenario 1). (c) Each client collects only the time series data from partial nodes but with complete knowledge about the network structure (Scenario 2). (d) Proposed FGNN framework for predicting network dynamics without compromising privacy.

The problem of predicting the network dynamics without compromising privacy is significantly more challenging than that of inferring the network structure, for the following three reasons. First, different clients record only partial time series data of (partial timestamps or partial nodes) of the network dynamics. Second, it is necessary to learn the rules of the dynamical evolution from the data. Third, the network data held by different clients are in general not iid (independently and identi-

cally distributed). To make the forecasting problem with full privacy protection addressable at the present, in this paper we focus on two data-collection scenarios. In Scenario 1, each client collects only the partial time series data of all nodes and the partial structure of networks, as illustrated in Fig. 1(b). In Scenario 2, each client has only the time series data from a subset of nodes, but each client has complete knowledge about the structure of the network, as shown in Fig. 1(c). We demonstrate that the prediction performance of the FGNN framework far exceeds that of the local models obtained by the individual local clients through local data. We also show that the FGNN framework is capable of predicting the evolution of a diverse array of discrete and continuous network dynamical processes. Overall, the FGNN framework represents a powerful machine-learning based approach to predicting the global network dynamics from only local data with guaranteed privacy protection.

II. THE PROPOSED FGNN FRAMEWORK

In this section, the architectures of the FGNN framework and its details are described.

A. Basic principle of proposed FGNN framework

Let $G = \{V, E\}$ denote a given network, where $V = \{v_i | i = 1, \dots, n\}$ and $E = \{e_{ij} | i, j = 1, \dots, n\}$ are the sets of nodes and edges, respectively. The available time series are organized into a data matrix \mathcal{X} , where each row corresponds to the time series of one node and each column is associated with one timestamp of all nodes. The data matrix \mathcal{X} is generated by an unknown dynamical process \mathcal{D} on the underlying network (In this work, four discrete and three continuous dynamics are considered, and detailed description of the various dynamical processes are presented in Sec. IV B in Appendix).

Let X^t be a vector that stores the states of all nodes at time t (i.e., a column of matrix \mathcal{X}), and the nodal state evolution over time t is given by

$$X^{t+1} = \mathcal{D}(X^t, G). \quad (1)$$

Suppose there are K clients and a client k views the network as its own local network structure G_k and the available time series data is denoted as \mathcal{X}_k (i.e., a sub-matrix of \mathcal{X}). The time series data of client k are expressed as $\mathcal{X}_k = \{X_k^1, \dots, X_k^{T_k}\}$, where T_k is the length of the time series recorded by client k . In Scenario 1, each client has partial timestamps of the whole time series data \mathcal{X} , and $X_k^t \in R^{n \times 1}$ denotes the states of all nodes at time t by client k . In Scenario 2, the time series data held by each client are at the same timestamp: $T_k = T, k = 1, 2, \dots, K$. Let V_k be the nodal set whose time series data can be observed by client k , where $X_k^t \in R^{|V_k| \times 1}$. The state of the node i at time t is expressed as $x_k^t(i) = (X_k^t)_i$.

Each client k can train a local machine learning model M_k to generate the network dynamics based on its own data, with a training parameter set denoted as θ_k . Because of the incomplete observation, the learning capability of any local model in capturing the network dynamics is limited. To overcome the limitation, we build up an FGNN framework by combining the information of $\{G_1, \dots, G_K\}$ and $\{\mathcal{X}_1, \dots, \mathcal{X}_K\}$ to train a global model M enabling us to better learn the dynamical process and to accurately predict the future nodal states of nodes. In particular, we have

$$M(X^t, G, \theta) \approx \mathcal{D}(X^t, G), \quad (2)$$

where θ denotes the parameter set of the global model.

The overall framework of FGNN is illustrated in Fig. 1(d), and it involves four main steps:

Step 1: The central unit initializes the model parameter set θ^0 and distributes them to each client.

Step 2: At the t th iteration, each client k uses the new parameter set θ^t to update its local model M_k . Each client k takes the current states X_k^t as the input at time t and outputs at the next time step the nodal states $\widehat{Y}_k^t = M_k(X_k^t, G_k, \theta_k^t)$ based on its own local network structure G_k . The real states used for training is $Y_t^k = X_{t+1}^k$. To train the model, the loss function of the local model is constructed by the real states and the output as

$$\mathcal{L}(\theta_k^t) = \frac{1}{|V_k|} \sum_{i \in V_k} L(y_k^t(i), \widehat{y}_k^t(i)), \quad (3)$$

where $L(y_k^t(i), \widehat{y}_k^t(i))$ is the loss function of node i between the real state and the predicted output. Once the loss function is defined, the parameter set θ_k^{t+1} of the local models can be updated by a standard back-propagation neural network model (see Sec. II B for further details).

Step 3: The updated parameters of all local models are sent to the central unit and the parameters of the global model θ is aggregated by the weights $\{\theta_1, \dots, \theta_K\}$ expressed as

$$\theta^{t+1} = \sum_{k=1}^K w_k \theta_k^{t+1}, \quad (4)$$

where w_k is the aggregation weight measuring the quality of the data of client k , and its details are given in Sec. II C. The new updated parameter set θ^{t+1} is sent back to each client.

Step 4: Repeating *steps 2-3* until the loss function converges or reaches a given number of training times, and the global FGNN model is the trained joint model.

B. Local model and loss functions

We use a three-layer neural network to construct the local model. To address that our framework can incorporate different GNN models, two widely used GNNs, i.e.,

the graph convolutional network (GCN) and the graph attention network (GATN) are used in the hidden layer. The input of the model is the nodal states data matrix \mathcal{X} . For discrete dynamics, one-hot coding is used as the inputs. For continuous dynamics, the continuous dynamical variables are taken directly as the inputs. The states of the nodes are embedded into a d -dimensional feature space through a linear layer $f_1 : R^S \rightarrow R^d$, where S denotes the dimension of the inputs. The second layer utilizes GCN or GATN to aggregate the information from the neighbors of a node. The model outputs the prediction \hat{Y} through a linear layer.

The output of the discrete dynamics is the normalized probability vector \hat{P}_i that the node i belongs to different discrete states, with the element $\hat{p}_{i,m}$ being the prediction probability of node i in the m -th state. The state with the highest probability in the vector is taken as the predicted state $\hat{y}(i)$ of node i . The cross entropy (CE) loss function is used for discrete dynamics, which is defined as

$$L_{CE}(P_i, \hat{P}_i) = - \sum_m p_{i,m} \log \hat{p}_{i,m}, \quad (5)$$

where P_i is the one-hot coding of the true state of node i and $p_{i,m}$ is the m th element of the vector.

The output of the continuous dynamics \hat{y} is a one-dimensional continuous variable. For continuous dynamics prediction, we use the mean square error (MSE) loss function:

$$L_{MSE}(y(i), \hat{y}(i)) = (y(i) - \hat{y}(i))^2. \quad (6)$$

The specific architectures of the neural networks for the discrete dynamics and continuous dynamics are summarized in Table I.

C. Weighted aggregation of parameters

We introduce a unified method to evaluate the quality of the local data. Assuming that the amount of time series data owned by each client k is $|D_k|$ and the amount of network structure data corresponds to the number of edges in it, denoted by $|E_k|$, we set the aggregation weight in model k as

$$w_k = \frac{1}{2} \left(\frac{|D_k|}{|D_1| + \dots + |D_K|} + \frac{|E_k|}{|E_1| + \dots + |E_K|} \right). \quad (7)$$

For Scenario 1, each client k has the time series data of all nodes at different timestamps (i.e., T_k) and the partial structure of the network (G_k). The aggregation weight in Eq. (4) can be rewritten as

$$w_k = \frac{1}{2} \left(\frac{T_k}{T_1 + \dots + T_K} + \frac{|E_k|}{|E_1| + \dots + |E_K|} \right). \quad (8)$$

For Scenario 2, all clients have the same network structure: $G_k = G$, $i = 1, 2, \dots, K$, so it is not necessary to consider the data quality. The length of time series data

in all clients is the same (the whole length of the original data), but each client only records the time series data on a subset of nodes. Consequently, the amount of data in each client k can be simply denoted as $|V_k|$, yielding

$$w_k = \frac{|V_k|}{|V_1| + \dots + |V_K|}. \quad (9)$$

D. Evaluation metrics

For discrete dynamics, we use the ACC index to measure the prediction accuracy, defined as

$$ACC = \sum_{i \in V_T} \frac{I(y(i) = \hat{y}(i))}{|V_T|}, \quad (10)$$

where $I(\cdot)$ is an indicator function and $|V_T|$ is the number of nodes in the test set V_T . A larger value of ACC indicates a higher prediction capability of the model.

For continuous dynamics, the differences between the true and predicted values of the dynamical variables are taken to be the prediction error. We choose two metrics to characterize the error: the mean square error (MSE) and the mean absolute percentage error (MAPE). In particular, we use MAPE to quantify the error for the mutualistic and gene dynamics. For CML dynamics, the values of the nodal dynamical variables are in the unit interval, and $y(i)$ is in the denominator of the MAPE metric. The value of MAPE can be large when $y(i)$ converges to zero, so we use the MSE metric for CML dynamics, where σ is defined as:

$$\sigma = \begin{cases} \frac{1}{|V_T|} \sum_{i \in V_T} \frac{|y(i) - \hat{y}(i)|}{y(i)}, & \text{Mutualistic/Gene,} \\ \frac{1}{|V_T|} \sum_{i \in V_T} (y(i) - \hat{y}(i))^2, & \text{CML.} \end{cases} \quad (11)$$

III. PERFORMANCE CHARACTERIZATION AND DEMONSTRATION

A. Generation of training data

First, the time series data of all nodes are generated by certain dynamics. If a dynamical process leads to a steady state, it is not possible to uncover the network dynamics. To ensure that sufficiently long time series data can be obtained, the states of nodes are re-initialized after some steps of evolution so as to prevent the states of nodes from entering any steady state. The states of the first timestamps are stored in the data matrix \mathcal{X} as the input of the model, and the next timestamps are stored in \mathcal{Y} as the real states of nodes. For each client, the time series data are generated by intercepting the original data. Specifically, in Scenario 1, each client uses the data of all nodes in different timestamps as the training set. In Scenario 2, each client records the whole length of the time series data on some nodes only, and the states of

TABLE I. Neural network architectures for discrete and continuous dynamics

	Discrete dynamics	Continuous dynamics
	One-hot (1, S)	Linear (1,32)
Input layer	Linear (S , 32) ReLU	ReLU
Hidden layer	GCN(32,32) or GATN (32,32) ReLU	GCN(32,32) or GATN (32,32) ReLU
Output layer	Linear (32, S) Softmax	Linear (32,1) ReLU
Loss function	Cross-Entropy Loss	Mean-Squared Loss

the missing nodes in the client are set as zero. This may lead to conflicts with the state of nodes for discrete dynamics. Our solution is to assign continuous values to the discrete states when training a discrete dynamics model in Scenario 2. By so doing, the model and train method are the same as for continuous dynamics. In addition, to reflect that each client only knows partial structure of the original network in Scenario 1, we randomly remove some edges following a uniform distribution.

B. Simulation settings of FGNN

To present our results in a concise and clear way, here in the main text we include results with the GCN (results with GATN are deferred to Sec. IV C in Appendix). Numerical experiments are performed on three synthetic networks (scale-free(BA), small-world(WS), and Erdős-Renyi (ER) random) and six real-world networks: Word [57], Celegans [58] (Cele), USAir [59], Metabolic [60] (Meta), Email [59], Tap [61] (see Sec. IV A in Appendix for the structural information of these networks).

For dynamical processes on networks, we use a diverse array of discrete and continuous dynamics to demonstrate the general applicability of our FGNN framework. In particular, we test four types of discrete dynamics (susceptible-infected-recovered (SIR) epidemic spreading dynamics [62], susceptible-infected-susceptible (SIS) dynamics [63], threshold dynamics [64], and Kirman dynamics [65]) and three types of continuous processes (i.e., gene regulatory dynamics (Gene) [66], mutualistic interaction dynamics among species in ecology (Mutualistic) [67], and coupled map lattices (CML) [68–70]). the detailed descriptions of these dynamical processes are summarized in Sec. IV B in Appendix.

In our simulations, the number of client is $K = 3$, where each client trains a local model individually based on the local data. The local models can be conveniently chosen as the baseline models, which are termed as Local_1, Local_2 and Local_3 for the three clients, respectively. A centralized model (termed as Center) is trained by using the full network structure and the full time se-

ries data. The model Center serves only the purpose of comparison, it has no privacy protection as it utilizes all information of the clients. Unless specified otherwise, the number of iterations for federated aggregation in our FGNN framework is set to be ten, and the learning rates of training the GCN and GATN models are 0.001 and 0.0001, respectively. The test set contains 20 time pairs ($t, t + 1$) of data. To reduce the statistical uncertainties, the values of the results are averaged over 20 realizations.

C. Results for simulated network dynamics

In our FGNN framework, a basic component is a centralized GNN. To demonstrate that GNNs are capable of predicting the network dynamics, we use the complete time series data and network structure to train the parameters in the GCN. The length of the time series in discrete dynamics is set as $T = 200$, and that for continuous dynamics is $T = 100$. In the trained GCN model, the nodal states at time T are then taken as the inputs with the states at time $T + 1$ as the prediction. Then, the predicted states at $T + 1$ are inputs to the model to yield the predicted states at $T + 2$, and so on. Table II presents the five-step prediction results of the GCN model on a scale-free network for time from $T + 1$ to $T + 5$. It can be seen that, for the four types of discrete dynamics, when the true states of nodes are inputted at T , the value of ACC at $T + 1$ is persistently larger than 80% (for the Kirman dynamics, the value is about 92%). Subsequently, when the predicted states are used as inputs, the ACC values somewhat decrease but they are still above 70% for the next five time steps. For the continuous dynamics, Table II shows the error σ between the predicted and true state values for time from $T + 1$ to $T + 5$.

The results from predicting the continuous dynamics indicate uniformly small prediction errors, regardless of the specific types of processes. The results in Table II thus demonstrate that the GCN model is capable of making accurate short-term state prediction for different types of network dynamical processes, paving the way for the model to be incorporated into our federated learning framework in which the prediction task is accomplished

TABLE II. Five-step prediction performance of GCN model - basic component of FGNN, for different types of network dynamics.

	Discrete dynamics (ACC)				Continuous dynamics (σ)		
	SIR	SIS	Threshold	Kirman	Gene	Mutualistic	CML
$T + 1$	0.87	0.85	0.80	0.92	0.672	1.168	0.025
$T + 2$	0.83	0.78	0.75	0.85	0.756	1.460	0.024
$T + 3$	0.78	0.75	0.73	0.83	0.820	1.647	0.024
$T + 4$	0.82	0.71	0.74	0.79	0.963	1.740	0.033
$T + 5$	0.80	0.70	0.72	0.81	1.001	1.718	0.030

by fusing data from different clients with their privacy fully protected.

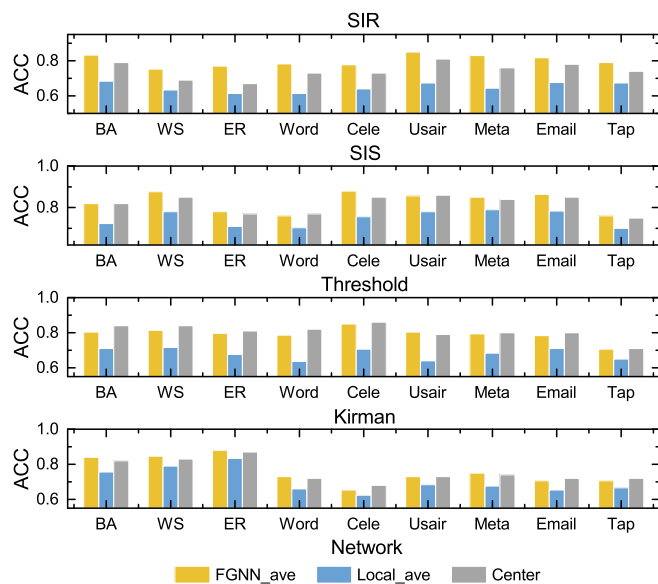


FIG. 2. Comparison of prediction performance of FGNN, local, and centralized models for discrete dynamics for Scenario 1. Shown are the average values of ACC from different models. The FGNN models significantly outperform the local models and demonstrate a similar performance level to that of the centralized model but with the desired advantage of full privacy protection.

We can now present the prediction results of our FGNN framework. For Scenario 1 of data collection, each client k has its own network structure G_k , which is not shared with others, leading to three global prediction models ($K = 3$), denoted as $FGNN_k = M(\mathcal{X}, \theta, G_k)$ for $k = 1, 2, 3$. For this case, the sampling probabilities of edges in the three clients are set as 80%, 60% and 50%, respectively. All clients are assumed to have the same nodal set, and the nodes without edges are treated as the isolated nodes. For the four types of discrete dynamics, the lengths of the time series in the three clients are set as 50, 30 and 20, respectively. For the three types of continuous dynamics, the lengths of time series data in the three clients are set as 20, 15 and 15, respectively. The three local models ($Local_k = M_k(X_k, \theta_k, G_k)$) and the centralized model (Center) serve as the baseline mod-

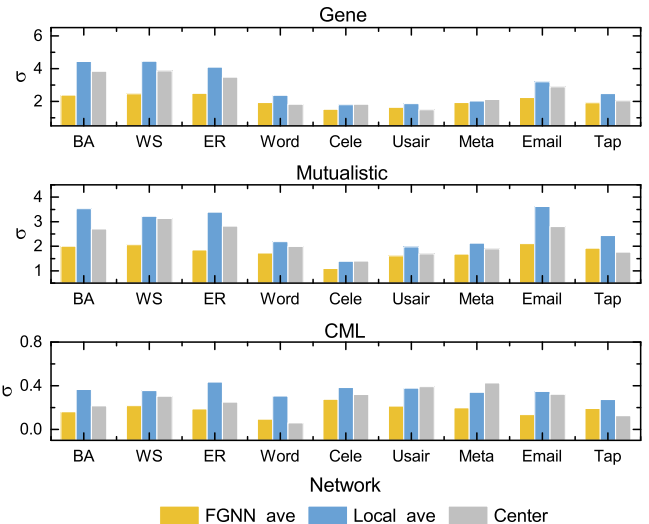


FIG. 3. Comparison of prediction performance of FGNN, local, and centralized models for continuous dynamics for Scenario 1. Shown are the average errors σ for different models. As for the case of discrete dynamics in Fig. 2, the FGNN models significantly outperform the local models and present a similar performance level to that of the centralized model but without compromising privacy.

els for comparison. For clarity, here we present the average results from the three FGNNs and three local models, denoted as $FGNN_{ave}$ and $Local_{ave}$, respectively.

Figure 2 shows, for data Scenario 1, the ACC values for the FGNN, local and the centralized models in predicting the discrete dynamics taking place on different networks. It can be seen that the FGNN models persistently outperform the local models in term of the ACC values, with similar or slightly better performance than that of the centralized model. Considering that there is no privacy protection in the centralized model as it requires complete time series data and complete information about the network structure, our FGNN models are desired as it offers full privacy protection. Figure 3 further compares the performance of different models in predicting the continuous network dynamics in terms of the measure σ , which again indicates that our FGNN framework gives significantly better prediction results than those from the local models and similar or slightly better results than the centralized model. The results in Figs. 2 and 3 thus

demonstrate that our FGNN framework can effectively combine multiple or fuse local data information to train a better global network dynamic model without disclosing the private data, regardless of the types of network dynamics and structure.

For data Scenario 2, different clients collect the time series data from a subset of nodes but each client possesses the same global network structure, so there is only one global federated learning model, denoted as $FGNN=M(\mathcal{X}, \theta, G)$. For this case, the length of the time series for the four types of discrete dynamics is set to be 50, and the length of time series data for the three types of continuous dynamics is set to be 20. In addition, the percentages of the nodes with data in the three clients are 70%, 80% and 80%, respectively. As we have mentioned in Sec. III B, for Scenario 2, we treat the discrete state as the continuous state to avoid the adverse consequence. Therefore, the MSE index is selected as the evaluation metric for the discrete network dynamics rather than the ACC index. Table III presents the prediction results of discrete network dynamics in term of MSE from different models. It can be seen that, in most cases the prediction results of our FGNN framework with privacy protection are better than those of the local models. For the centralized model, in spite of its use of the complete data, the prediction performance is not significantly better than that of our FGNN framework. Table IV illustrates the prediction results for the three types of continuous dynamics from different models. Similar to the results in Table III, our FGNN model can better predict the true nodal states than the local models and, in some cases, even outperforms the centralized model.

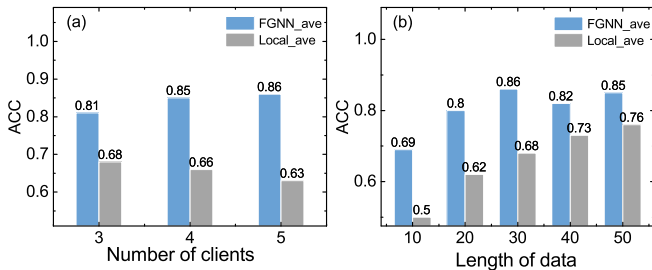


FIG. 4. Impacts of the number of clients (a) and the length of time series (b) on the prediction performance for different models. The dynamical process is of the SIR type, the network is of the scale-free type, and data collection follows Scenario 1. In all cases, our FNGG model yields significantly better results than the local models.

To further demonstrate the robustness of our FGNN framework, we study the impacts of the number of clients and the length of time series data on the prediction performance. To be illustrative, we consider Scenario 1 and use the SIR dynamics on scale-free networks. Figure 4(a) shows the effect of the number of clients, for $K = 3$ (the sampling probabilities of edges are 80%, 60%, 50%, and the length of the time series are 50, 30, 20), $K = 4$ (the sampling probabilities of edges are 80%, 60%, 50%, 60%,

and the length of the time series are 50, 30, 20, 15) and $K = 5$ (the sampling probabilities of edges are 80%, 60%, 50%, 60% and 50%, and the length of the time series are 50, 30, 20, 15, 10). As the number of clients increases, the performance of the local models decreases, as each client possesses less information, i.e., fewer time series data points and less structural information about the network. In contrast, with more clients, our FGNN models yields increasingly better performance - an intrinsic feature of federated learning in general. Figure 4(b) presents the effect of the time series length on the prediction performance for the case of $K = 3$, where the length for each client is the same for each simulation (10, 20, 30, 40 and 50). There is no overlapping in the data for different clients. For example, if the total length of the time series is $T = 30$ and there are three clients, we set the data length for each client to be 10. The sampling probabilities of edges in the three clients are set as 80%, 60% and 50%, respectively. It can be seen from Fig. 4(b) that the ACC values from our FGNN model are persistently higher than those from the local models for all cases. For shorter time series, the advantage of our FGNN model is more pronounced. As expected, as the data length increases, the prediction performance of the local models is improved as each client has more data to train the neural network.

D. Results for real-world network dynamics: predicting influenza evolution

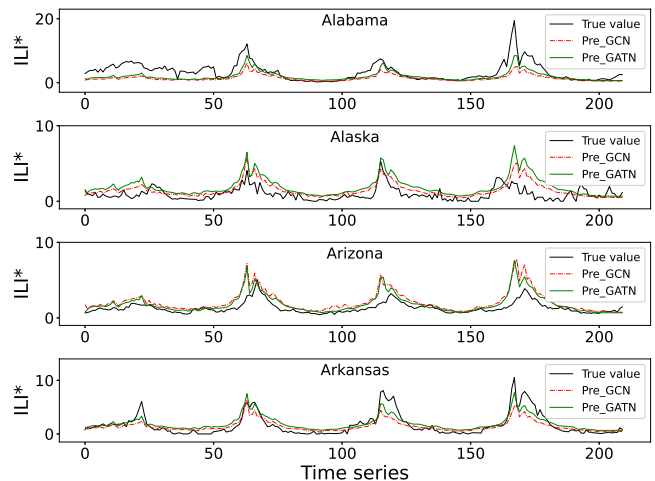


FIG. 5. Performance of two types of GNNs (without privacy protection) in predicting the evolution of the influenza spreading in four States in the US. The black, red dotted and green curves are the ground truth, and the predicted ILI* values are GCN (Pre_GCN) and GATN (Pre_GATN).

We further apply our FGNN framework for predicting the dynamical states to a real-world problem: outbreak of influenza. The time series are from the US weekly

TABLE III. For Scenario 2, prediction performances of different models in term of MSE for four types of discrete dynamics for synthetic and real-world networks. The best performance in each row is highlighted in bold.

Dynamic Method	SIR			SIS			Threshold			Kirman		
	FGNN	Local	Lave	Center	FGNN	Local	Lave	Center	FGNN	Local	Lave	Center
Scale-free	1.371	1.560	1.495	0.923	1.533	1.216	0.654	4.627	1.531	0.992	5.487	4.402
Small-world	1.111	1.619	1.530	0.818	1.331	1.065	0.449	0.767	0.473	0.432	0.924	0.466
ER random	1.328	1.768	1.654	1.024	1.341	1.311	0.663	1.972	1.279	0.722	1.012	0.790
Word	2.243	3.549	2.229	1.218	2.380	1.651	0.416	0.656	0.557	0.363	0.386	0.386
Cele	1.629	2.232	1.430	1.309	2.193	1.688	0.331	0.367	0.330	0.526	0.458	0.436
USAir	1.879	3.085	1.716	1.291	1.538	1.271	0.465	0.981	0.502	0.458	0.612	0.514
Meta	1.358	1.220	1.241	1.276	1.645	1.106	0.516	0.596	0.507	0.860	1.815	0.468
Email	1.255	2.042	1.666	1.140	1.522	1.058	0.422	0.535	0.514	0.463	0.594	0.494
Tap	1.206	1.215	1.370	1.452	1.722	1.437	0.501	0.878	0.779	0.633	0.839	0.918

TABLE IV. For Scenario 2, prediction performances of different models in term of σ for three types of continuous dynamics for synthetic and real-world networks. The best performance in each row is highlighted in bold.

Dynamic Method	Gene			Mutualistic			CML					
	FGNN	Local	Lave	Center	FGNN	Local	Lave	Center	FGNN	Local	Lave	Center
Scale-free	1.165	1.432	1.406	1.245	1.781	1.480	0.529	0.839	0.426			
Small-world	1.331	1.714	1.648	1.815	2.419	1.941	0.358	0.990	0.356			
ER random	0.797	0.878	0.766	1.577	1.847	1.616	0.648	0.888	0.395			
Word	0.800	1.046	0.870	1.113	1.275	1.223	0.538	0.959	0.581			
Cele	0.889	1.448	0.793	1.574	2.003	2.098	0.404	0.878	0.416			
USAir	1.230	1.393	1.415	1.619	2.192	2.240	0.481	0.829	0.645			
Meta	1.402	1.323	1.076	1.992	1.967	1.719	0.462	0.702	0.477			
Email	1.161	1.480	1.289	1.522	2.152	1.886	0.298	0.325	0.281			
Tap	1.322	1.540	1.587	2.372	2.921	2.779	0.413	1.376	1.279			

TABLE V. MSE values of the global FGNN model and the baseline models under data Scenario 1 in predicting the evolution of influenza in four States in the US.

	MSE	FGNN_1	FGNN_2	FGNN_3	Local_1	Local_2	Local_3	Center
GCN	1.591	1.642	1.570	1.678	1.756	1.741	1.594	
GATN	0.685	0.814	0.822	1.413	1.394	1.506	1.271	

TABLE VI. MSE values from the global FGNN and the baseline models under data Scenario 2 in predicting the evolution of influenza in four States in the US.

MSE	FGNN	Local_1	Local_2	Local_3	Center
GCN	1.600	1.622	2.584	2.499	1.852
GATN	1.227	1.646	1.352	1.808	1.684

influenza-like illness (ILI) data base [71] for the five-year time period from the 40th week of 2011 to the 39th week of 2016, which records the weekly number of ILI-related visits to all public health and clinical laboratories in the country by the CDC (Center for Disease Control). For data pre-processing, we normalize the weekly ILI-related visits in each State to calculate the ILI ratio, i.e., the percentage of the patients with influenza among all visiting patients in each State [72]. We then use the data values in which the percentage of the ILI ratio is removed to represent the state of the underlying dynamical system, record as ILI*. The underlying network supporting

the influenza spreading across the different States in the US is identified by taking advantage of the commuting traffic data in different States in 2015 to generate a population commuting network among the States [73]. The raw data are available from the website of the USA Bureau of Statistics, and the commuting data among the States are obtained by aggregating the raw data (A detailed description of data processing and the data settings are provided in Sec. IV D in Appendix).

As for the various cases of synthetic dynamic data treated in the preceding subsection, the first step is to validate the effectiveness of the GNNs. For this purpose, we use the influenza data at the *previous time steps* to train the GNNs. The trained GNNs and the ILI* of nodes (i.e., states) at the *current time step* are the inputs for predicting the trend of the influenza at the *next time step*. Figure 5 shows the true and the predicted values in term of ILI* for the first four States in the alphabetic list of the US States. It can be seen that the predicted values fit well the real evolution of the influenza in these

States, and the peaks of the influenza at several representative time points (i.e., outbreaks) can also be predicted. The results in Fig. 5 thus demonstrate that the predicted dynamics can fit the evolution of the influenza to a satisfactory extent.

Having demonstrated the performance of the two GNNs, we can proceed to test the predictive power of our FGNN framework and that of the baseline methods with respect to the two data scenarios. The number of clients is set to be $K = 3$. For data Scenario 1, partial timestamps of all nodes are collected and the information about the structure of the commuting network is incomplete. For Scenario 2, the time series data of partial nodes are used. Table V shows, for Scenario 1, the MSE values associated with the FGNN predictions with the GCN and GATN models, the local models and the centralized model. Regardless of whether the global model is GCN or GATN, our FGNN models of the three clients (FGNN_1, FGNN_2, FGNN_3) can achieve better prediction performance than those of the local models (Local_1, Local_2, Local_3) and the centralized model (Center). Table VI summarizes the MSE values for the FGNN and baseline methods for Scenario 2. It can be seen that our global FGNN model also yields significantly better prediction results than those of the baseline models. For both data scenarios, Tables V and VI unveil a surprising result: the prediction performance of the FGNN model exceeds that of the centralized model that uses the complete data (and so does not offer any data privacy protection). A plausible reason is that our FGNN framework relies an iterative process and so it has more training time and yields a better learning model.

IV. DISCUSSION

In our modern time, time series data generated from network dynamical processes and the underlying structure of the network are typically owned by different parties. There are two possible data distribution scenarios that are amenable to simulations and analysis at the present: Scenario 1 in which different clients have the data timestamps of all nodes but each client has only partial information about the structure of the network, and Scenario 2 in which different clients have the data from only a subset of nodes in the network but each client has the full knowledge of the network structure. To combine multi-party data to better predict network dynamics while protecting privacy of the clients is a problem of great importance and interest. We have proposed an FGNN framework to address this problem. The essence of our prediction framework is to combine the data from different clients to jointly train a high-quality global model without disclosing any private data. The framework is compatible with existing GNNs to learn network dynamics and predict the states of nodes into the near future. We have used two classical GNN models (GCN and GATN) to demonstrate the power and effec-

tiveness of our FGNN framework through extensive numerical simulations of a good number of synthetic and real-world networks as well as a variety of discrete and continuous network dynamics. Our systematic comparison of the performances of our global FGNN model, baseline local and centralized models under different conditions reveals that the global model learned through the FGNN framework has superior accuracy in predicting the dynamical evolution of the network and is thus capable of better capturing the complex relationship between dynamics and network structure. The impacts of the number of clients and the length of time series data on the dynamics prediction have been investigated, revealing the general applicability and robustness of our FGNN framework.

A practically significant contribution of our work is the demonstration of successful prediction of the evolutionary trend of influenza in the US by our articulated FGNN framework without compromising privacy. In particular, any State in the US is regarded as a node in the network which we have reconstructed using the State-crossing commuting data, and the short-term dynamical evolution of the influenza spreading dynamics on this network has been predicted. Our results indicate that, not only is the FGNN framework capable of reproducing the actual time evolution of the influenza in the States, but the outbreaks (corresponding to peaks of the dynamical evolution) can also be faithfully predicted.

The two data scenarios treated in this paper are somewhat specific. A more general scenario is that each client has partial time series data from a subset of nodes and incomplete information about the network structure. To predict the dynamical evolution of the network without compromising data privacy under this general scenario is an open question warranting further investigation.

ACKNOWLEDGMENTS

The authors are grateful to Drs. Wen Hu and Xiao Ding for helpful discussions. We also thank Dr. Sen Pei for sharing the website of the influenza data in the USA. This work is supported by National Natural Science Foundation of China (Grant No. 61973001) and by The University Synergy Innovation Program of Anhui Province (Grant No. GXXT-2021-032). The work at Arizona State University was supported by AFOSR under Grant No. FA9550-21-1-0438.

APPENDIX

A. Structural information of networks

Experiments are performed on three synthetic networks and six real-world networks. The sizes of the synthetic networks are 100 nodes. In particular, the scale-free (BA) networks are generated with $m = 2$, where m is

TABLE VII. Basic structural information of six real networks.

Network	n	M	$\langle k \rangle$	CC	H
Word	112	425	7.589	0.173	1.815
Celegans	297	2148	14.465	0.292	1.801
USAir	332	2126	12.807	0.749	3.464
Metabolic	453	2025	8.940	0.647	4.485
Email	1133	5451	9.622	0.220	1.942
Tap	1373	6833	9.953	0.529	1.644

the number of edges connecting to the existing nodes at each preferential attachment step. The small-world (WS) network are generated with the average degree $\langle k \rangle = 4$ and reconnection probability $p = 0.3$. The Erdős-Renyi (ER) random networks are generated with the edge connection probability $p = 0.08$. The structural information of the six real-world networks is summarized in Table VII, where n and M are the numbers of nodes and edges of the network, respectively, CC is the clustering coefficient, $H = \langle k^2 \rangle / \langle k \rangle^2$ is the network heterogeneity, and $\langle k^2 \rangle$ is the second moment of the degree distribution.

B. Seven types of network dynamics

We describe the four types of discrete and three types of continuous networked dynamical processes used in our study, in our paper, which all have been well studied to gain insights into a variety of network phenomena in natural or social sciences.

SIR dynamic model. In the SIR model [62], at any time a node can be in one of three states: susceptible (S), infectious (I) and recovery (R). The I -state node can infect its S -state neighbors with the infection rate λ . If an infection event is successful, the infected node will change its state from S to I ; Otherwise it will remain in the S state. The infected nodes will recover to the R state with the recovery rate μ , and the R -state nodes will not be infected again. In our study, the parameter values are set as $\lambda = 0.2$ and $\mu = 0.1$. The states of all nodes are randomly initialized after every ten time steps.

SIS dynamic model. In the SIS model [63], there are two distinct dynamical states only: S and I . An I -state node can infect its susceptible neighbors with the infection rate λ and recover to the S state with the recovery rate μ . In our study, the parameter values are set as $\lambda = 0.2$ and $\mu = 0.1$. The states of all nodes are randomly initialized after every ten time steps.

Threshold dynamic model. In the threshold model [64], nodes can be in one of the two states: inactive (0) and active (1). An inactive node is activated when the fraction of its active neighbors is greater than an activation threshold of the node, and an active node will be not restored again. In our study, the activation threshold for all node is set to be 0.5, and the states of all nodes are re-initialized after every five time steps.

Kirman dynamic model. In the Kirman model [65], a node can be in one of the two states: 0 and 1. The transition between the two states is based upon two transfer functions. In particular, the transfer function of the node from 0 to 1 is given by $c_1 + dm_1$, and that from 1 to 0 is $c_2 + d(k - m_1)$, where c_1 and c_2 quantify the individual behavior of the node that is independent of neighbors' state, and k is the nodal degree, d describes the probability of node replicating a neighbor's state, and m_1 is the number of 1-state neighbors. In our study, the parameters are set as $c_1 = 0.1$, $c_2 = 0.1$ and $d = 0.08$.

The continuous networked dynamics employed in our study are one-dimensional with the state variable $x_i(t) \in R$ for node i at time t . The states of all nodes at time t can be represented by the vector $X(t) = [x_1(t), \dots, x_n(t)]^T \in R^n$. The differential equations governing the three types of continuous dynamics in our study are as follows.

Gene regulatory dynamics (Gene). The gene regulation dynamics are expressed by the Michaelis Menten equation [66]:

$$\frac{dx_i(t)}{dt} = -u_i x_i(t) + \sum_{j=1}^n A_{ij} \frac{(x_j(t))^h}{(x_j(t))^h + 1}, \quad (12)$$

where the first item controls the decay of the current node state, u_i is the decay rate, and the second term captures gene activation characterized by the Hill coefficient h . We use $u_i = 1$ and $h = 2$. The states of all nodes are re-initialized after 50 time steps.

Mutualistic interaction dynamics (Mutualistic). The differential equations governing the evolution of mutualism in ecological systems [67, 74] are

$$\frac{dx_i(t)}{dt} = u_i + x_i(t) \left(1 - \frac{x_i(t)}{l_i}\right) \left(\frac{x_i(t)}{z_i} - 1\right) + \sum_{j=1}^N A_{ij} \frac{x_i(t)x_j(t)}{\alpha_i + \beta_i x_i(t) + \gamma_i x_j(t)}, \quad (13)$$

where the first item u_i represents the number of migrating individuals of species i from the adjacent habitat, the second item l_i describes the carrying capacity of the system growth, and z_i is the cold-start threshold. When the abundance of species i is low (i.e., $x_i(t) < z_i$), the system is characterized by a negative growth. The third item in Eq. (13) describes the interactions among the species, which take place on a network described by the adjacency matrix \mathcal{A} . In our study, we use the parameter values $u_i = 0.1$, $l_i = 5$, $z_i = 1$, $\alpha_i = 5$, $\beta_i = 0.9$, and $\gamma_i = 0.1$. The states of all nodes are re-initialized after each 50 time steps.

Coupled map lattices (CML). In a coupled mapping lattice, the continuous state variables are updated at discrete time [68–70] according to

$$x_i(t+1) = (1-s)f(x_i(t)) + \frac{s}{k_i} \sum_{j=1}^N A_{ij} f(x_j(t)), \quad (14)$$

where s is the coupling parameter (the system degenerates into a set of independent mapping functions for

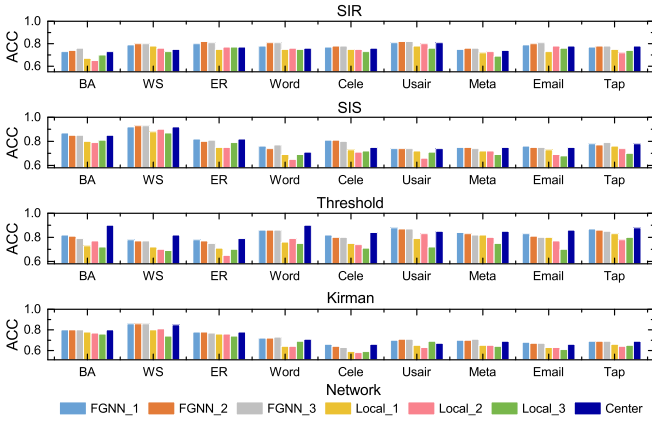


FIG. 6. FGNN/GATN model performance. Shown are the values of ACC from the global models and the baseline methods for the four types of discrete dynamical processes under data Scenario 1.

$s = 0$) and k_i is the degree of node i . In our study, we use the mapping function $f(x) = \lambda x(1 - x)$ for the parameters $\lambda = 3.5$ and $s = 0.2$. The states of all nodes are re-initialized after each 50 time steps.

C. GATN simulation results

We present the detailed simulation results of the GATN-based FGNN model and the local model of each client. Table VIII verifies the good performance of the GATN model in predicting the four discrete dynamics ($T = 200$ for GATN training) and the three continuous dynamics ($T = 100$ for GATN training) with the complete time series data and the complete network structure (for scale-free networks). Figure 6 shows the values of ACC from the FGNN global models and the baseline methods for the four types of discrete dynamics under data Scenario 1. Figure 7 shows the prediction results for the three types of continuous dynamics, which also suggest that the FGNN global models have lower prediction errors than those of the local models. For data Scenario 2, the results in Table IX demonstrate that the performance of our FGNN method in predicting the four types of discrete dynamics is persistently better than that of the local models. Table X shows the results of different methods in predicting the three types of continuous dynamics. In most cases, the prediction results of our FGNN method are closer to the real values than those from the local models.

D. Influenza data

1. Description of influenza data

The influenza-like illness (ILI) data used in our study are from the US public health and clinical laborato-

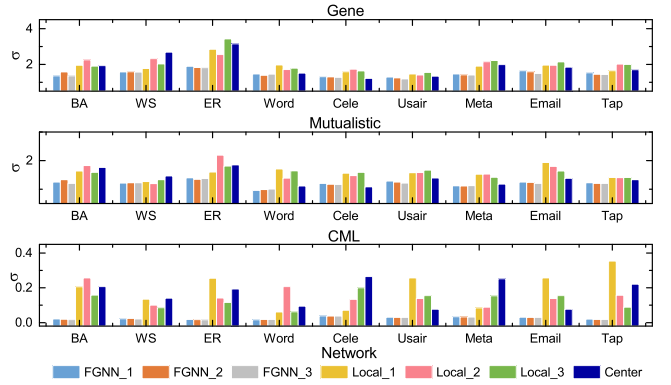


FIG. 7. FGNN/GATN model performance. Shown are the prediction error σ from the global models and the baseline methods for the three types of continuous dynamical processes under data Scenario 1.

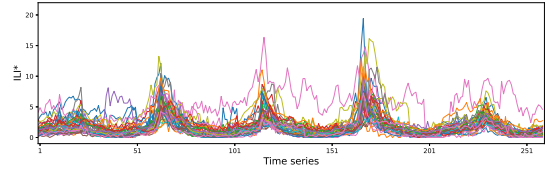


FIG. 8. Real ILI* values in the 37 States from the 40th week of 2011 to the 39th week of 2016.

ries [71], which were collected weekly from the 40th week of 2011 to the 39th week of 2016. We standardize the weekly ILI data by using the number of visiting patients in each State in the US to calculate the ILI ratio [72]. In order to ensure a sufficient sample size in the data, we assume that the States whose average weekly ILI ratio is less than 1% are not representative. Accordingly, 14 States are removed. The remaining 37 States are listed in Table XI. Because the small value of ILI ratio (about 2%) can lead to errors, we multiply the ILI ratio by the factor of 100 (labelled as ILI*) and use the resulting values the dynamic data. The curves of ILI* for the 37 States are shown in Fig. 8.

Population commuting between the States is the key to spreading dynamics. We use the commuting data in the USA by residential geography to construct the commuting network. The commuting data between the USA cities are from the 2015 census report [73]. The State level commuting data are calculated by aggregating the city data, leading to a State-level commuting network for the 37 States. The network is directed and weighted, where the nodes represent the States and the edges are determined by the commuting data among the States. To prevent the network from being too dense, we use the criterion that, if the number of commuters between the two states is less than 100, the corresponding edge is removed. The resulting network has 763 directed edges. Finally, we use the min-max normalization procedure [75] to obtain the weights of the edges by dividing the number

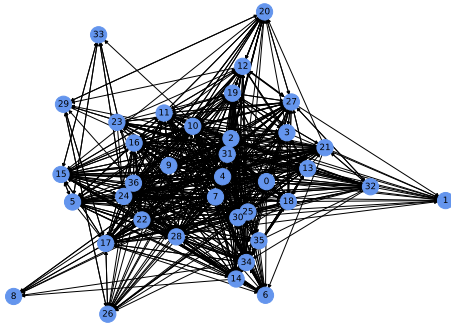


FIG. 9. The directed and weighted network constructed from the commuting data among the 37 US States.

of commuters by the maximum number of commuters. The constructed directed and weighted network can be

visualized, as shown in Fig. 9, where the thickness of the directed edges denotes the weight.

2. Simulation settings of influenza data

Under Scenario 1, the first 100 data points are selected from a total of 260 ILI* data points. The numbers of data assigned to the three clients are 50, 30 and 20, respectively, and the network structures for the three clients are generated by sampling 90%, 80% and 70% of edges from the commuting network. The learning rates of the FGNN/GCN and FGNN/GATN models are set to be 0.0001 and 0.001, respectively. Under data Scenario 2, the first 50 data points are selected from a total of 260 ILI* data points. The percentages of nodes with the influenza data for the three clients are 80%, 70% and 60%, respectively. The learning rates of the GCN and GATN models are set as 0.01 and 0.0001, respectively.

-
- [1] W.-X. Wang, Y.-C. Lai, and C. Grebogi, *Phys. Rep.* **644**, 1 (2016).
- [2] H. Wang, C. Ma, H.-S. Chen, Y.-C. Lai, and H.-F. Zhang, *Nature Communications* **13**, 1 (2022).
- [3] D. Yu, M. Righero, and L. Kocarev, *Phys. Rev. Lett.* **97**, 188701 (2006).
- [4] D. Zhou, Y. Xiao, Y. Zhang, Z. Xu, and D. Cai, *Phys. Rev. Lett.* **111**, 054102 (2013).
- [5] M. Timme, *Phys. Rev. Lett.* **98**, 224101 (2007).
- [6] M. Timme and J. Casadiego, *J. Phys. A: Math. Theo.* **47**, 343001 (2014).
- [7] M. Nitzan, J. Casadiego, and M. Timme, *Sci. Adv.* **3** (2017).
- [8] C. Ma, H.-F. Zhang, and Y.-C. Lai, *Phys. Rev. E* **96**, 022320 (2017).
- [9] X. Li and X. Li, *Nat. Commun.* **8**, 15729 (2017).
- [10] W.-X. Wang, R. Yang, Y.-C. Lai, V. Kovanis, and C. Grebogi, *Phys. Rev. Lett.* **106**, 154101 (2011).
- [11] W.-X. Wang, R. Yang, Y.-C. Lai, V. Kovanis, and M. A. F. Harrison, *EPL (Europhys. Lett.)* **94**, 48006 (2011).
- [12] Z.-S. Shen, W.-X. Wang, Y. Fan, Z. Di, and Y.-C. Lai, *Nat. Commun.* **5**, 4323 (2014).
- [13] R.-Q. Su, Y.-C. Lai, and X. Wang, *Entropy* **16**, 3889 (2014).
- [14] G. Mei, X. Wu, Y. Wang, M. Hu, J.-A. Lu, and G. Chen, *IEEE Trans. Cybernet.* **48**, 754 (2018).
- [15] Y.-C. Lai, *Chaos* **31**, 082101 (2021).
- [16] W.-Y. Lin, Y.-H. Hu, and C.-F. Tsai, *IEEE Trans. Sys. Man Cybernet. C (Appl. Rev.)* **42**, 421 (2011).
- [17] L.-W. Kong, H.-W. Fan, C. Grebogi, and Y.-C. Lai, *Phys. Rev. Research* **3**, 013090 (2021).
- [18] L.-W. Kong, H.-W. Fan, C. Grebogi, and Y.-C. Lai, *J. Phys. Complex.* **2**, 035014 (2021).
- [19] N. Kumar and M. Raubal, *Transport. Res. C Emerg. Tech.* **133**, 103432 (2021).
- [20] J. D. Farmer and J. J. Sidorowich, *Phys. Rev. Lett.* **59**, 845 (1987).
- [21] M. Casdagli, *Physica D* **35**, 335 (1989).
- [22] G. Gouesbet, *Phys. Rev. A* **44**, 6264 (1991).
- [23] T. Sauer, *Phys. Rev. Lett.* **72**, 3811 (1994).
- [24] E. Baake, M. Baake, H. G. Bock, and K. M. Briggs, *Phys. Rev. A* **45**, 5524 (1992).
- [25] U. Parlitz, *Phys. Rev. Lett.* **76**, 1232 (1996).
- [26] J. P. Crutchfield and B. McNamara, *Complex Sys.* **1**, 417 (1987).
- [27] E. M. Bollt, *Int. J. Bif. Chaos* **10**, 1033 (2000).
- [28] C. Yao and E. M. Bollt, *Physica D* **227**, 78 (2007).
- [29] E. Candès, J. Romberg, and T. Tao, *IEEE Trans. Info. Theory* **52**, 489 (2006).
- [30] E. Candès, J. Romberg, and T. Tao, *Comm. Pure Appl. Math.* **59**, 1207 (2006).
- [31] W.-X. Wang, Y.-C. Lai, C. Grebogi, and J.-P. Ye, *Phys. Rev. X* **1**, 021021 (2011).
- [32] M. Raissi, *J. Mach. Learn. Res.* **19**, 932 (2018).
- [33] J. Pathak, B. Hunt, M. Girvan, Z. Lu, and E. Ott, *Phys. Rev. Lett.* **120**, 024102 (2018).
- [34] J. Pathak, A. Wilner, R. Fussell, S. Chandra, B. Hunt, M. Girvan, Z. Lu, and E. Ott, *Chaos* **28**, 041101 (2018).
- [35] A. Griffith, A. Pomerance, and D. J. Gauthier, *Chaos* **29**, 123108 (2019).
- [36] T. Qin, K. Wu, and D. Xiu, *J. Comp. Phys.* **395**, 620 (2019).
- [37] Z. Zhang, Y. Zhao, J. Liu, S. Wang, R. Tao, R. Xin, and J. Zhang, *Appl. Net. Sci.* **4**, 1 (2019).
- [38] H. Fan, J. Jiang, C. Zhang, X. Wang, and Y.-C. Lai, *Phys. Rev. Research* **2**, 012080 (2020).
- [39] C. Zhang, J. Jiang, S.-X. Qu, and Y.-C. Lai, *Chaos* **30**, 083114 (2020).
- [40] C. Zhang and F. Wang, in *Proceedings of the 26th ACM SIGKDD International Conference on Knowledge Discovery & Data Mining* (2020) pp. 892–902.
- [41] J. Z. Kim, Z. Lu, E. Nozari, G. J. Pappas, and D. S. Bassett, *Nat. Mach. Intell.* **3**, 316 (2021).
- [42] S. J. Mooney and V. Pejaver, *Ann. Rev. Pub. Health* **39**, 95 (2018).
- [43] K. Yu, L. Tan, X. Shang, J. Huang, G. Srivastava, and P. Chatterjee, *IEEE Consum. Electro. Mag.* **10**, 111

- (2020).
- [44] L. Lenert and B. Y. McSwain, *J. Ame. Med. Info. Asso.* **27**, 963 (2020).
- [45] M. J. Atallah and W. Du, in *Workshop on Algorithms and Data Structures* (Springer, 2001) pp. 165–179.
- [46] M.-L. Zhang and Z.-H. Zhou, *IEEE Trans. Knowle. Data Eng.* **26**, 1819 (2013).
- [47] J. Konečný, H. B. McMahan, D. Ramage, and P. Richtárik, arXiv preprint arXiv:1610.02527 (2016).
- [48] M. Yurochkin, M. Agarwal, S. Ghosh, K. Greenewald, N. Hoang, and Y. Khazaeni, in *International Conference on Machine Learning* (PMLR, 2019) pp. 7252–7261.
- [49] Y. Liu, J. James, J. Kang, D. Niyato, and S. Zhang, *IEEE Internet of Things Journal* **7**, 7751 (2020).
- [50] C. Wu, F. Wu, Y. Cao, Y. Huang, and X. Xie, arXiv preprint arXiv:2102.04925 (2021).
- [51] F. Sattler, S. Wiedemann, K.-R. Müller, and W. Samek, *IEEE Trans. Neu. Net.Learn. Sys.* **31**, 3400 (2019).
- [52] G. Mei, Z. Guo, S. Liu, and L. Pan, in *2019 IEEE International Conference on Big Data* (IEEE, 2019) pp. 2560–2568.
- [53] C. He, K. Balasubramanian, E. Ceyani, C. Yang, H. Xie, L. Sun, L. He, L. Yang, P. S. Yu, Y. Rong, *et al.*, arXiv preprint arXiv:2104.07145 (2021).
- [54] Q. Yang, Y. Liu, T. Chen, and Y. Tong, *ACM Trans. Intel. Sys. Tech.* **10**, 1 (2019).
- [55] C. Chen, W. Hu, Z. Xu, and Z. Zheng, arXiv preprint arXiv:2105.03170 (2021).
- [56] B. McMahan, E. Moore, D. Ramage, S. Hampson, and B. A. y Arcas, in *Artificial Intelligence and Statistics* (PMLR, 2017) pp. 1273–1282.
- [57] M. E. Newman, *Phys. Rev. E* **74**, 036104 (2006).
- [58] D. J. Watts and S. H. Strogatz, *Nature* **393**, 440 (1998).
- [59] R. Guimera, L. Danon, A. Diaz-Guilera, F. Giralt, and A. Arenas, *Physical Review E* **68**, 065103 (2003).
- [60] J. Duch and A. Arenas, *Phys. Rev. E* **72**, 027104 (2005).
- [61] A. Zeng and C.-J. Zhang, *Phys. Lett. A* **377**, 1031 (2013).
- [62] B. Shulgin, L. Stone, and Z. Agur, *Bull. Math. Biol.* **60**, 1123 (1998).
- [63] M. R. Sanatkar, W. N. White, B. Natarajan, C. M. Scoglio, and K. A. Garrett, *IEEE Trans. Sys. Man Cybernet. Sys.* **46**, 345 (2015).
- [64] W. Chen, Y. Yuan, and L. Zhang, in *2010 IEEE International Conference on Data Mining* (IEEE, 2010) pp. 88–97.
- [65] A. Kirman, *Quar. J. Econo.* **108**, 137 (1993).
- [66] A. Ocone, L. Haghverdi, N. S. Mueller, and F. J. Theis, *Bioinformatics* **31**, i89 (2015).
- [67] J. Jiang, Z.-G. Huang, T. P. Seager, W. Lin, C. Grebogi, A. Hastings, and Y.-C. Lai, *Proc. Nat. Acad. Sci. (USA)* **115**, E639 (2018).
- [68] K. Kaneko, *Prog. Theor. Phys.* **74**, 1033 (1985).
- [69] K. Kaneko and I. Tsuda, *Complex Systems: Chaos and Beyond, a Constructive Approach with Applications in Life Sciences* (Springer, Berlin, 2000).
- [70] Z. Zhang, Y. Zhao, J. Liu, S. Wang, R. Tao, R. Xin, and J. Zhang, *Appl. Net. Sci.* **4**, 1 (2019).
- [71] “The ILI data of USA,” [Online], available: <https://gis.cdc.gov/grasp/fluview/fluportaldashboard.html/>.
- [72] S. Pei, S. Kandula, W. Yang, and J. Shaman, *Proc. Nat. Acad. Sci. (USA)* **115**, 2752 (2018).
- [73] “The county-to-county commuting data of USA,” [Online], available: <https://www.census.gov/data/tables/2015/demo/metro-micro/co>
- [74] J. Gao, B. Barzel, and A.-L. Barabási, *Nature* **530**, 307 (2016).
- [75] S. Patro and K. K. Sahu, arXiv Preprint 1503.06462 (2015).

TABLE VIII. Five-step dynamics prediction results of GATN model based on complete time series data and complete network structure.

	Discrete dynamics(ACC)				Continuous dynamics(σ)		
	SIR	SIS	Threshold	Kirman	Gene	Mutualistic	CML
$T + 1$	0.85	0.86	0.89	0.84	0.598	0.958	0.017
$T + 2$	0.73	0.80	0.84	0.81	0.602	1.086	0.021
$T + 3$	0.81	0.75	0.81	0.82	0.609	1.276	0.024
$T + 4$	0.82	0.74	0.74	0.83	0.724	1.512	0.027
$T + 5$	0.80	0.74	0.72	0.85	0.822	1.601	0.028

TABLE IX. Values of MSE from the global and baseline models for the four types of discrete dynamics for FGNN/GATN under data Scenario 2.

Dynamic Method	SIR					SIS					Threshold					Kirman				
	FGNN	Local_1	Local_2	Local_3	Center	FGNN	Local_1	Local_2	Local_3	Center	FGNN	Local_1	Local_2	Local_3	Center	FGNN	Local_1	Local_2	Local_3	Center
Scale-free	0.843	0.846	0.862	0.893	0.865	0.177	0.286	0.484	0.533	0.261	0.413	0.477	0.456	0.418	0.427	0.249	0.435	0.269	0.255	0.259
Small-world	0.897	1.022	1.034	1.046	1.220	0.146	0.170	0.144	0.201	0.136	0.245	0.245	0.282	0.375	0.311	0.259	0.323	0.285	0.315	0.342
ER random	0.649	0.638	0.696	0.674	0.655	0.242	0.310	0.253	0.237	0.211	0.224	0.245	0.266	0.273	0.302	0.242	0.298	0.277	0.327	0.265
Word	0.699	0.799	0.917	0.763	0.791	0.249	0.255	0.269	0.494	0.249	0.295	0.538	0.268	0.442	0.341	0.251	0.277	0.265	0.265	0.271
Cele	0.496	0.512	0.511	0.498	0.478	0.270	0.282	0.278	0.272	0.257	0.301	0.346	0.387	0.347	0.316	0.254	0.309	0.307	0.266	0.317
USAir	0.699	0.744	0.820	0.747	0.716	0.246	0.249	0.347	0.363	0.252	0.401	0.474	0.572	0.456	0.419	0.251	0.266	0.265	0.433	0.250
Meta	0.681	0.793	0.813	0.695	0.735	0.232	0.254	0.248	0.29	0.250	0.311	0.335	0.286	0.540	0.290	0.251	0.289	0.314	0.317	0.283
Email	0.696	0.750	0.765	0.731	0.771	0.251	0.290	0.298	0.286	0.284	0.257	0.446	0.301	0.350	0.759	0.251	0.399	0.269	0.279	0.290
Tap	0.632	0.669	0.675	0.662	0.701	0.253	0.322	0.248	0.294	0.254	0.250	0.305	0.262	0.284	0.245	0.246	0.316	0.321	0.257	0.347

TABLE X. Values of prediction error from the global and baseline models for the three types of continuous dynamics for FGNN/GATN under data Scenario 2.

Dynamic Method	Gene					Mutualistic					CML				
	FGNN	Local_1	Local_2	Local_3	Center	FGNN	Local_1	Local_2	Local_3	Center	FGNN	Local_1	Local_2	Local_3	Center
Scale-free	1.160	1.163	1.159	1.627	1.122	1.741	1.834	1.437	1.733	1.636	0.123	0.199	0.162	0.245	0.192
Small-world	1.258	1.351	1.255	1.120	1.139	1.141	1.295	1.382	1.184	1.264	0.156	0.237	0.213	0.217	0.313
ER random	0.774	0.823	0.788	0.811	0.743	1.349	1.341	1.372	1.177	1.308	0.191	0.354	0.249	0.174	0.101
Word	0.774	1.019	0.916	1.201	0.884	1.655	1.624	1.646	1.754	1.442	0.229	0.197	0.235	0.287	0.146
Cele	0.686	0.844	0.857	1.035	0.778	1.005	1.202	1.250	1.580	1.316	0.176	0.169	0.200	0.161	0.172
USAir	0.891	1.018	1.009	1.097	0.945	1.165	1.420	1.341	1.395	1.361	0.146	0.155	0.198	0.170	0.148
Meta	0.990	1.080	1.072	1.180	1.006	1.245	1.394	1.407	1.490	1.481	0.151	0.267	0.191	0.183	0.088
Email	1.261	1.044	1.086	1.212	1.055	1.310	1.626	1.409	1.583	1.489	0.085	0.123	0.168	0.067	0.053
Tap	0.955	1.040	0.969	1.038	0.908	1.207	1.310	1.411	1.317	1.234	0.093	0.176	0.137	0.122	0.109

TABLE XI. Names of the 37 US States used in our study.

Alabama	Alaska	Arizona	Arkansas	California	Connecticut	Columbia
Georgia	Hawaii	Idaho	Illinois	Indiana	Kansas	Louisiana
Maryland	Massachusetts	Michigan	Minnesota	Mississippi	Missouri	Nebraska
Nevada	New Jersey	New Mexico	New York	North Carolina	North Dakota	Oklahoma
Pennsylvania	South Dakota	Tennessee	Texas	Utah	Vermont	Virginia
West Virginia	Wisconsin					